

Rotman Lens Design with Wideband DRA Array

Mohammad Ranjbar Nikkhah^{1, *}, Manish Hiranandani², and Ahmed A. Kishk³

Abstract—For rapid Rotman lens design, the symmetry plane is utilized to reduce the structure size by employing the odd and even mode characteristics. Solutions of half the structure for odd and even modes (short and open walls or electrical and magnetic walls, respectively) are much more efficient than the one-time solution for the whole structure. Then, s -parameters from both solutions are processed to obtain the s -parameters of the full lens. To support the wideband and wide scanning range, DRA array is used because of its ability to support these characteristics. Two examples are considered. The first example that employs four cylindrical DRA elements is built and measured to test the concept of terminating the dummy ports by absorbing materials instead of matching loads. This termination tremendously simplifies the structure and reduces the cost by saving the terminating connectors and the matching loads. Here, thin planar absorbing material is used on top of the microstrip lines of the dummy ports. The simulated and measured results are in good agreement. The second example utilizes 8 rectangular DRA array elements and is studied numerically.

1. INTRODUCTION

Rotman lens is a true-time delay beamformer, which has been extensively investigated via geometrical optics over the past decades [1]. Beams produced by Rotman lenses are relatively fixed in the entire operating band and do not vary significantly with frequency. These attractive features make Rotman lens the best candidate for multi-beam phased array antennas. Rotman lens is an elegant answer to generate multiple beams because of its low profile, broad bandwidth, low price, and comfort of its construction [2]. Since the lens was invented in 1963 [1], many researchers have proposed several designs and applications. Developing a microstrip Rotman lens design was reported in 1967 [3]. Furthermore, Rotman lens on a dielectric slab to reduce conductor losses has been reported [4]. Rectangular waveguide ports have also been used for Rotman lenses [5]. However, impedance bandwidth and possible scanning view range are limited [4, 5]. The purpose of a three-dimensional stack of Rotman lenses feeding a planar array antenna to generate beams with hexagonal lattice has been described [6]. Rotman lens can be utilized as a device for real-time microwave/millimeter-wave imaging as high-quality images from near-field targets have been achieved [7]. Lately, faster design of the Rotman lens based on odd and even mode characteristics was presented [8].

Dielectric resonator antennas (DRAs) have several attractive advantages such as small size, high radiation efficiency, and wide impedance bandwidth with no surface waves [9, 10]. Phased array antennas with DRA elements have been described [10]. Rotman-DRA phased arrays are suitable combinations to achieve a wide scanning range of the wideband phased array antenna. Recently, a low cost phased array with DRA elements based on ESPAR (Electronically Steerable Parasitic Array Radiator) theory and inexpensive reactive loads were reported [11, 12]. Until nowadays, little attention is given to DRA phased array [13].

Received 8 May 2020, Accepted 10 October 2020, Scheduled 12 December 2020

* Corresponding author: Mohammad Ranjbar Nikkhah (ranjbar.nik@gmail.com).

¹ University of Wisconsin-Madison, USA. ² Intel Corporation, USA. ³ Concordia University, Canada.

Here, first, a fast technique for Rotman lens design based on E- and H-wall symmetrical planes (like odd and even modes or open and short walls, respectively) is introduced. Rotman lens for large array and many beams within a broad view range (wide scanning range) is a considerable numerical structure. It is a challenging design problem based on full-wave analysis to develop its accurate s -parameters. Thus, an efficient design process is required. Here, we propose a simple procedure that is verified by two examples. Array factors based on the measured and simulated S -parameters are compared. Then, a study on the wide-scan view of a Rotman-DRA phased array is described.

2. PROCEDURE FOR DESIGN

Rotman lens design is well established. Their original equations have been explained [6]. The typical design consists of three parts: a lens body, capturing horns with delay lines, and the antenna array. The lens body is formed by the beam curve and array curve. The durations of the delay lines from the array curve to the antenna array are controlled to have three perfect focal points. A designer can work out the length of the delay line from the design equations of the lens-based mainly on the chosen design parameters (scan angle, central angle, the ratio of on-axis to off-axis focal length, and the electric properties of the dielectric substrate).

The essential design equations for Rotman lens are based on ray-optical modeling. Ray-optical modeling is not accurate for wideband Rotman lens designs because of the reflections off the side walls (where dummy ports are made) and the coupling among the horn opening to the feed lines as they are not considered in the ray-optics part. It should be noted that in our design, Rotman lens, beam and array curves, and port directions are developed by geometrical optics (GO) analysis, and then sidewall contours (curve of dummy ports) are modified to minimize the multiple reflections from the side walls. Multiple reflections significantly decrease if the dummy port's reflections are pointing to the center of the array ports and beam ports contours. Moreover, the orientations of the dummy ports in the sidewalls are very crucial in the design of Rotman lens, which should be optimized rigorously.

By getting the lens profile using GO, beam port profile, array port profile, and port directions are determined. Then, proper capturing horns are attached to the beam and array sides of the lens with an opening width based on the required number of ports and the length of the lens profile for each side. Here, we use printed circuit technology. Therefore, the horn output width is established by the microstrip line width that will be linked to it. The horn length is based on the required length that transforms the horn opening impedance to the microstrip line impedance. After finalizing these geometries, the structure is ready for the full-wave analysis using the commercial software Microwave Studio CST [14].

2.1. Theory

To reduce the runtime for getting the s -parameters of the lens, E- and H-wall symmetrical planes (like odd and even modes) are considered, as shown in Fig. 1 as an example for the illustration of 11 ports. Let us generalize the situation by considering that the total number of beam ports and antenna ports and not counting the dummy ports is $N = M + L$, where M and L are the numbers of beam and antenna ports, respectively. The beam ports are numbered $1, 2, \dots, M$, and the antenna ports are numbered $M + 1, M + 2, \dots, N$. If M is an even number, then $M/2$ ports are above the symmetry line. If M is an odd number, then $(M - 1)/2$ are above the symmetry line, and port $(M - 1)/2 + 1$ is a split port by the symmetry line. Similarly, for the antenna ports, for even number, $L/2$ ports are above the symmetry line, and for odd number $(L - 1)/2$ ports are above the symmetry line. Port $M + (L - 1)/2 + 1$ is a split port by the symmetry line. Now, for the beam ports $S(l, l) = S(k, k)$, (l is the image of k), $k = 1, 2, \dots, [M/2]$ for even or $[(M - 1)/2]$ for odd, and $l = M + 1 - k$. For the antenna ports, $S(l, l) = S(k, k)$, (l is the image of k), $k = M + 1, M + 2, \dots$ to $[M + L/2]$ for even or $[M + (L - 1)/2]$ for odd number of beam ports and $l = N + 2L - k$. Now, $S(k, l) = S(k', l')$ where k is the image of k' , and l is the image of l' .

In addition, due to the reciprocity, $S(k, l)$ is equal to $S(l, k)$ where k is not equal to l . Therefore, it is sufficient to get $S(k, k)$ for the ports above the symmetry line to know $S(k, k)$ for all ports. Also, $S(k, l)$ is calculated where k is for the ports above the symmetry and l for all ports.

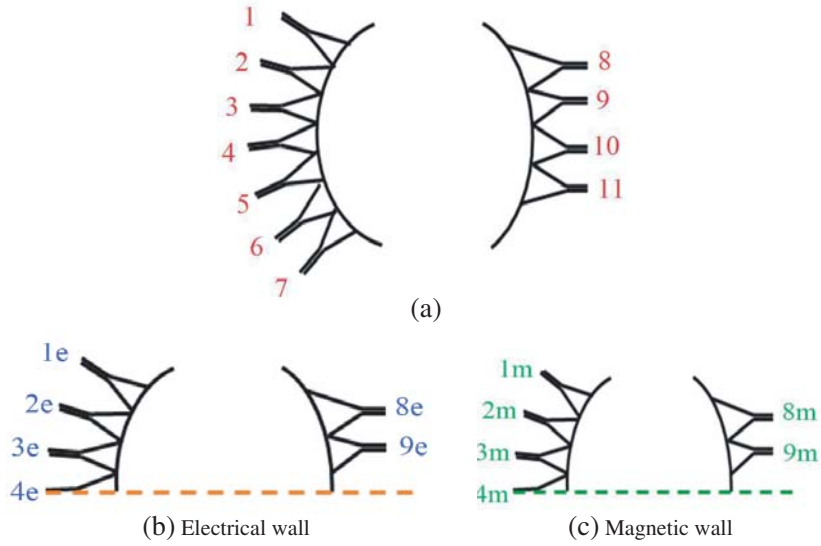


Figure 1. Sketch of Rotman lens: (a) original Rotman lens, (b) half structure with E -plane symmetric condition, and (c) half structure with H -plane symmetric condition.

Using symmetry and reciprocity all transmission between the ports will be known.

The reflection coefficients of the original Rotman lens are given by Equation (1) for the ports above the symmetric line. If the port is on the symmetry line, the reflection coefficient is obtained from the summation of Equations (1) and (2). Equations (3) and (4) are for the transmission between the ports on the same side of the symmetry line and the ports of the opposite sides of the symmetry line, respectively. If k and l lie on the same side of the symmetric line of the lens, Equation (3) is used, and if k and l lie on the opposite sides of the symmetric line, Equation (4) should be employed. Since Rotman lens has a challenging design procedure and to obtain the best outcomes, a full-wave solution is necessary for various tests. So, this technique helps to speed Rotman lens design significantly.

$$S(k, k) = \frac{Sm(k, k) + Se(k, k)}{2} \tag{1}$$

$$S(k, k) = \frac{Sm(k, k) - Se(k, k)}{2} \tag{2}$$

$$S(k, l) = \frac{Sm(k, l) + Se(k, l)}{2} \tag{3}$$

$$S(k, l) = \frac{Sm(k, l') - Se(k, l')}{2} \tag{4}$$

where Sm and Se are the S -parameters in the case of using the half structure with a magnetic wall and electric wall, respectively. In Fig. 1, $N = 11$, $M = 7$, and $L = 4$. Therefore, if the port splits such as port 4, we add Eqs. (1) and (2) for $S(4, 4)$ and add Eqs. (3) and (4) for $S(k, 4)$.

3. LENS DESIGN

To try the concept, a Rotman lens is designed based on the explanation in Section 2. An in-house MATLAB code based on the GO design is utilized to provide the beam and array profiles lengths. The horns are added to them based on the pre-specified number of ports. The output of the GO-MATLAB code is presented, as shown in Fig. 2 to five array ports and six beam ports (odd number to have a beam in the broadside direction). It should be mentioned that $F/D = 1$ is chosen, and also the focal angle parameter is set equal to the maximum scan angle. The proposed lens is fabricated on a 20 mil Rogers 5880. The dimensions of the prototype Rotman lens are $30 \times 40 \text{ cm}^2$, as can be seen in Fig. 2. The maximum scan angle is $\pm 38^\circ$. Input and output reflection coefficients for 50Ω ports are plotted in

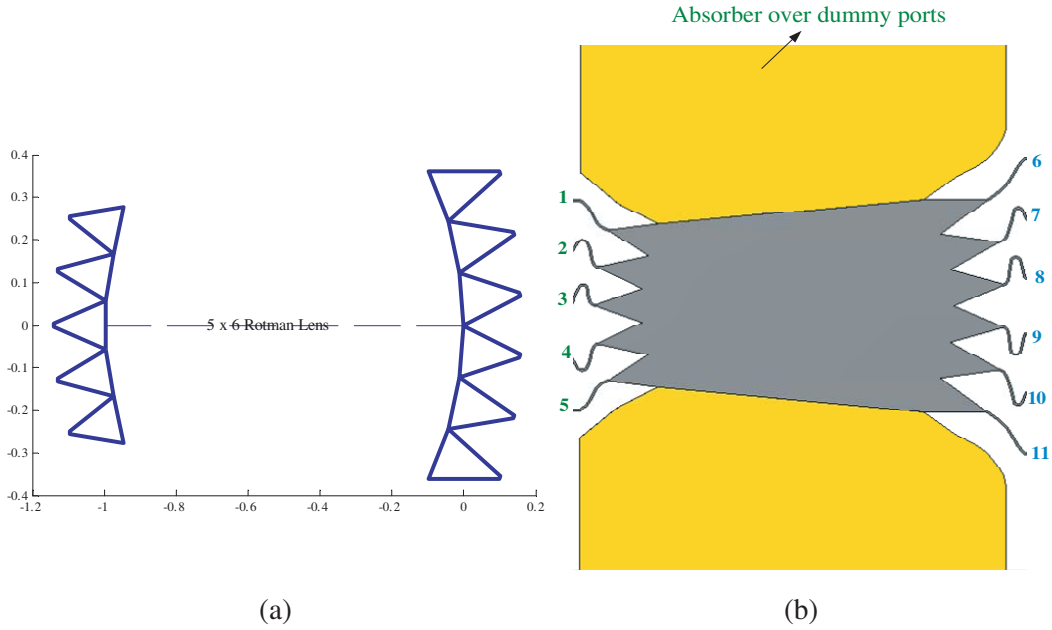


Figure 2. (a) Rotman lens configuration based on geometrical optics MATLAB in-house code (including beam and array port directions), (b) a 5×6 Rotman lens Full-wave modeled in CST software (absorber is modeled by $\epsilon = 12$, $\mu = 1.2$, electric tand = 0.2, magnetic tand = 1.2, and thickness = 3 mm).

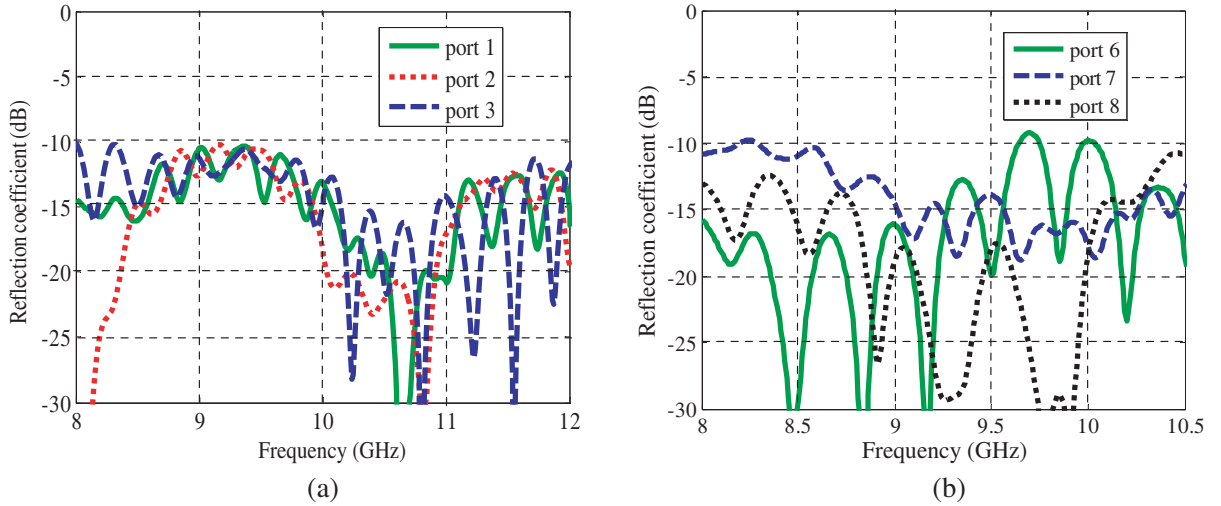


Figure 3. Full-wave simulated reflection coefficient: (a) beam ports of Rotman lens, (b) array ports of the Rotman lens.

Figs. 3(a) and (b), respectively. Looking at the coupling diagrams, S_{ij} , we should furnish the required level and melt off the potential losses to avoid scan losses. Measured and simulated coupling diagrams are plotted in Fig. 4 for beam ports (ports 1, 2, and 3) to array ports. The power is distributed with reasonable power tapering over the entire frequency band. It is interesting to point out that instead of using absorber material, dummy ports should be terminated with 50 Ohms matched loads. There is not much difference in the s -parameters when absorber materials or matched loads are used with the dummy ports, as can be seen in Fig. 5. Absorber material provides a smoother variation of the S -parameters versus frequency. Then, from the measured s -parameters, the array factors are plotted

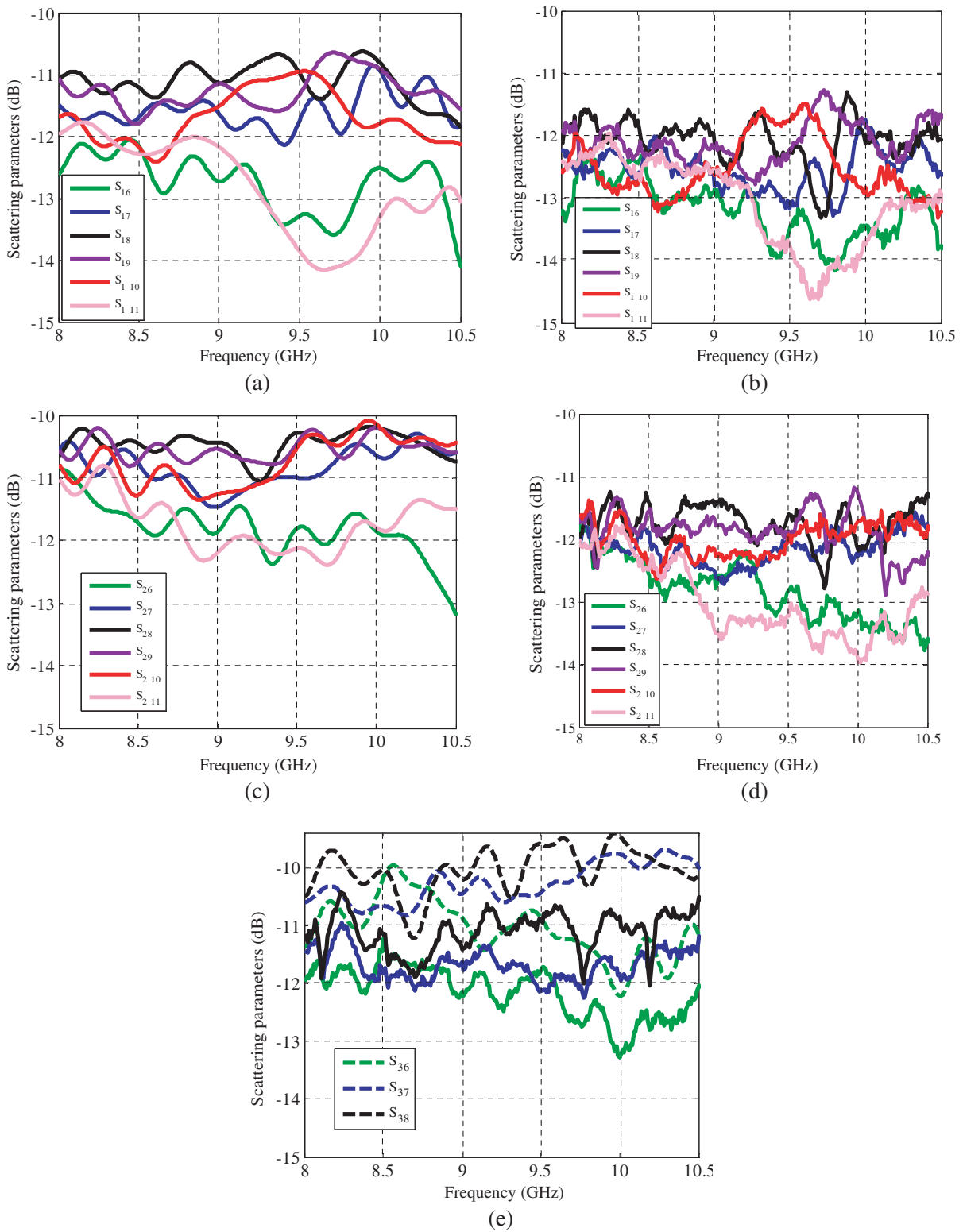


Figure 4. Measured and full-wave simulated coupling diagram for the proposed Rotman lens: (a) beam port 1 to array ports (simulated), (b) beam port 1 to array ports (measured), (c) beam port 2 to array ports (simulated), (d) beam port 2 to array ports (measured), and (e) beam port 3 to array ports (solid line: measured, dash line: simulated).

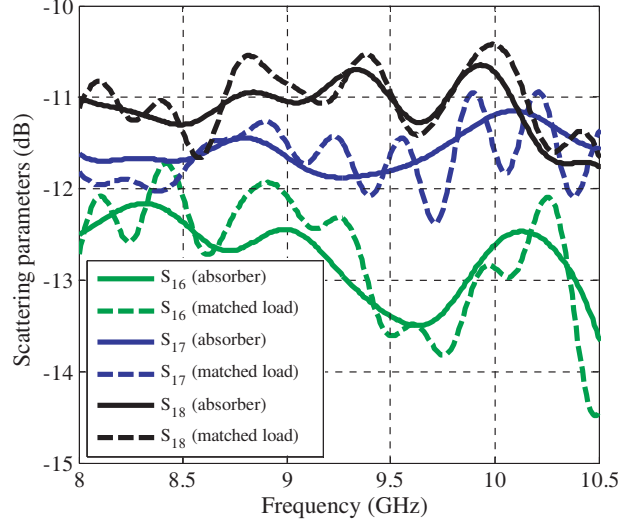


Figure 5. Full-wave simulated scattering parameters. (solid line: absorber is placed on dummy ports, dashed line: dummy ports are terminated with 50 Ohm matched loads).

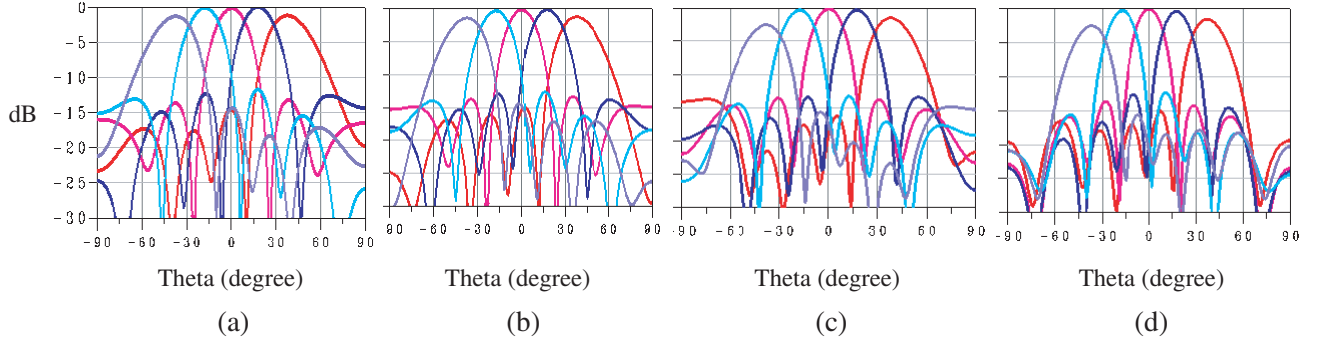


Figure 6. Measured array factors based on measured S -parameters for the proposed Rotman lens (output element spacing = 15 mm): (a) 8 GHz, (b) 8.5 GHz, (c) 9.5 GHz, and (d) 10.5 GHz (y -axis is in dB scale, and all the figures share the same y -axis of the left figure).

considering element spacing of 15 mm. The measured array factors at different frequencies are plotted, as shown in Fig. 6. These results show stable beam-scanning directions within the scanning frequency range. The array factors based on measured S -parameters for the proposed Rotman lens can be written in a general form for a lens with N beam ports and M array ports. The array factor due to exciting the beam port l is given in Equation (5) with d being the distance between the array elements.

$$|AF_l| = \sum_{i=N+1}^{M+N} |S_{il}| e^{j(\angle S_{ik} - \mathbf{k} \cdot \mathbf{r}_i)} \quad (5)$$

where \mathbf{k} is the wavenumber, and \mathbf{r}_i is the element position vector.

4. DRA ROTMAN PHASED ARRAY

In this section, we provide a linear dielectric resonator antenna array fed by a Rotman lens. Two examples of Rotman-DRA are reported.

4.1. Example 1

A wideband aperture coupled cylindrical DRA element is designed based on [15]. A linear array based on this element is designed. The center to center element spacing is 15 mm. In the second step, a 7×4 Rotman lens is designed in the X-band. The substrate with $\epsilon_r = 2.2$ (Taconic's TLY-5A-0100) is chosen for the design. The Rotman-DRA is fabricated and tested, as presented in Fig. 7. It should be mentioned that instead of using matched loads terminating the dummy ports, an absorber (MCS/SS6M from Emerson & Cuming Microwave Products) is used to cover the extended microstrip transmission lines of the dummy ports to absorb the signal while it is traveling under these lines. The simulated reflection coefficients for beam ports of the proposed Rotman lens are presented in Fig. 8. The simulated coupling diagrams from beam ports (1, 2, 3, and 4) to array ports (8, 9, 10, and 11) are shown in Figs. 9(a), (b), (c), and (d), respectively. Measured radiation patterns are presented in Fig. 10, and the reflection coefficients for the phased array are shown in Fig. 11. The performance of the proposed design is compared with the published results in the literature in Table 1.

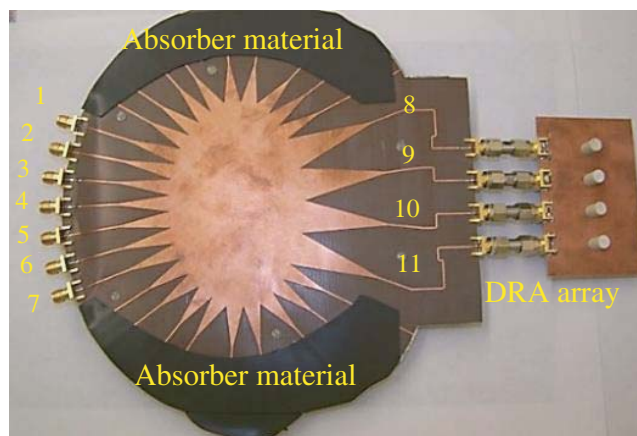


Figure 7. Fabricated Rotman-RDA array (7×4 Rotman lens) with dummy ports are coated with absorbing materials.

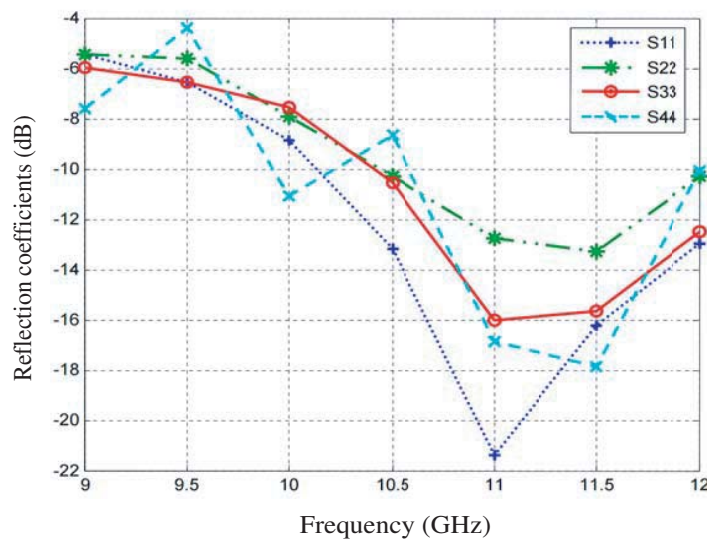


Figure 8. The Simulated reflection coefficients from the beam ports.

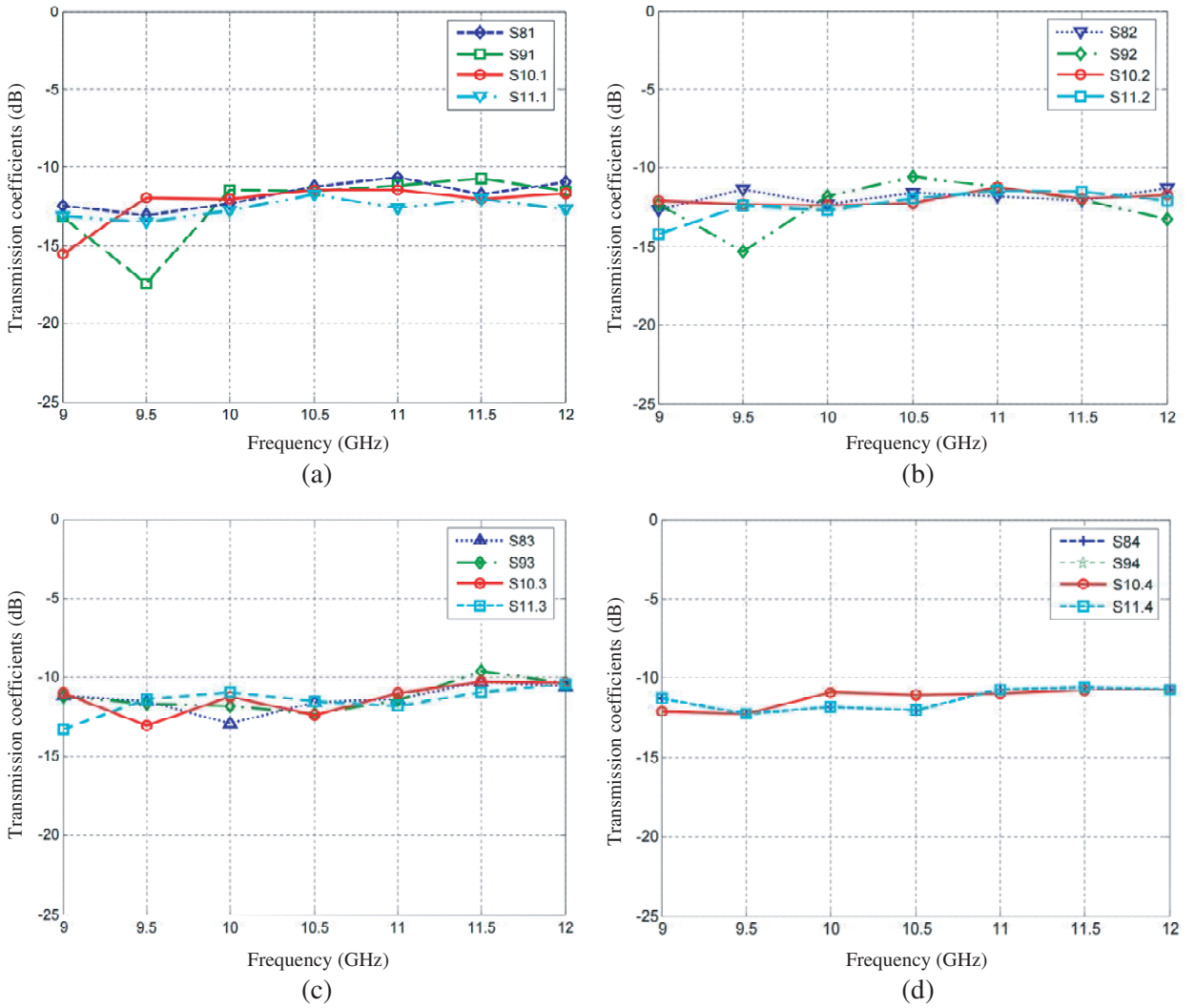


Figure 9. The simulated Coupling diagrams for the proposed Rotman lens: (a) beam ports 1 to array ports, (b) beam port 2 to array ports, (c) beam port 3 to array ports, (d) beam port 4 to array ports.

Table 1. Comparison between our work and other previously reported in literature.

	Rotman Phased array antenna element Type	Frequency (GHz)	Beam scanning (degrees)	Scan loss (dB)
[16]	Substrate integrated waveguide	24.15 (single)	± 33	1.65
[17]	Substrate integrated waveguide	28.5 (single)	± 40	5
[18]	Series fed microstrip array	24 (single)	± 28	5
[19]	Vivaldi	8–12	± 40	2.5
This work	DRA	9.5–12	± 45	2

4.2. Example 2

In this section, a wider band DRA (6–11 GHz) is selected and also a Rotman lens with more beam ports (11) and array ports (8) with a scanning range of $\pm 37^\circ$ is designed as shown in Fig. 12. Full-wave

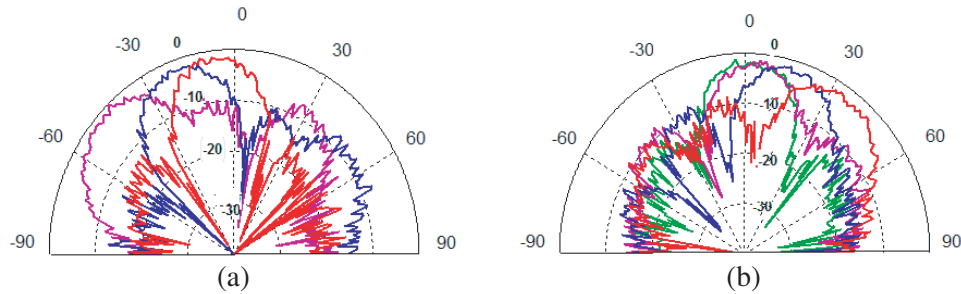


Figure 10. Measured radiation patterns for the Rotman-DRA phased array antenna for different beam ports at 10 GHz. (a) Left Figure: radiation patterns for beam 1 (purple), 2 (blue) and 3 (red). (b) Right Figure: Radiation patterns for beam 4 (green), 5 (purple), 6 (blue) and 7 (red).

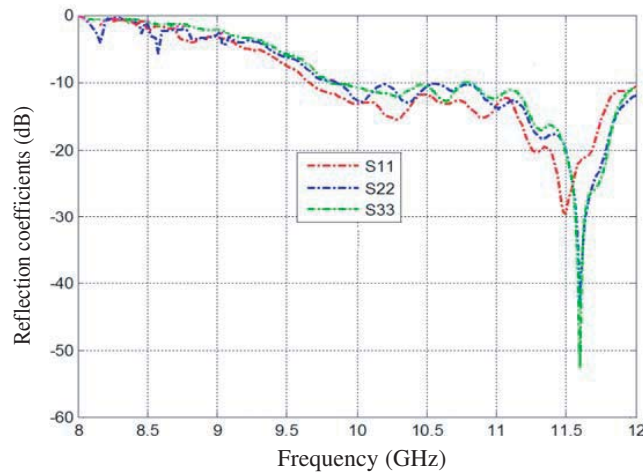


Figure 11. Measured reflection coefficients for the beam ports of the structure in Fig. 7.

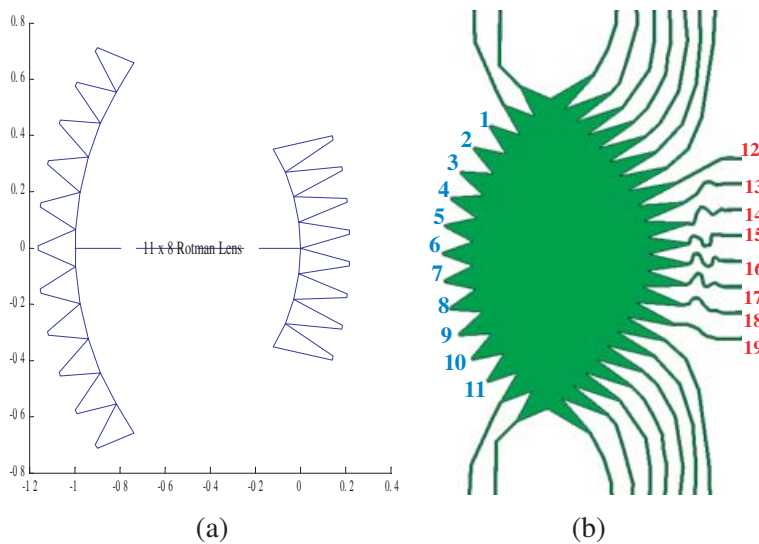


Figure 12. Rotman lens configuration: (a) based on geometrical optic MATLAB in-house code (including Input and output Rotman curves, input and output ports direction), (b) Full-wave simulated Rotman structure.

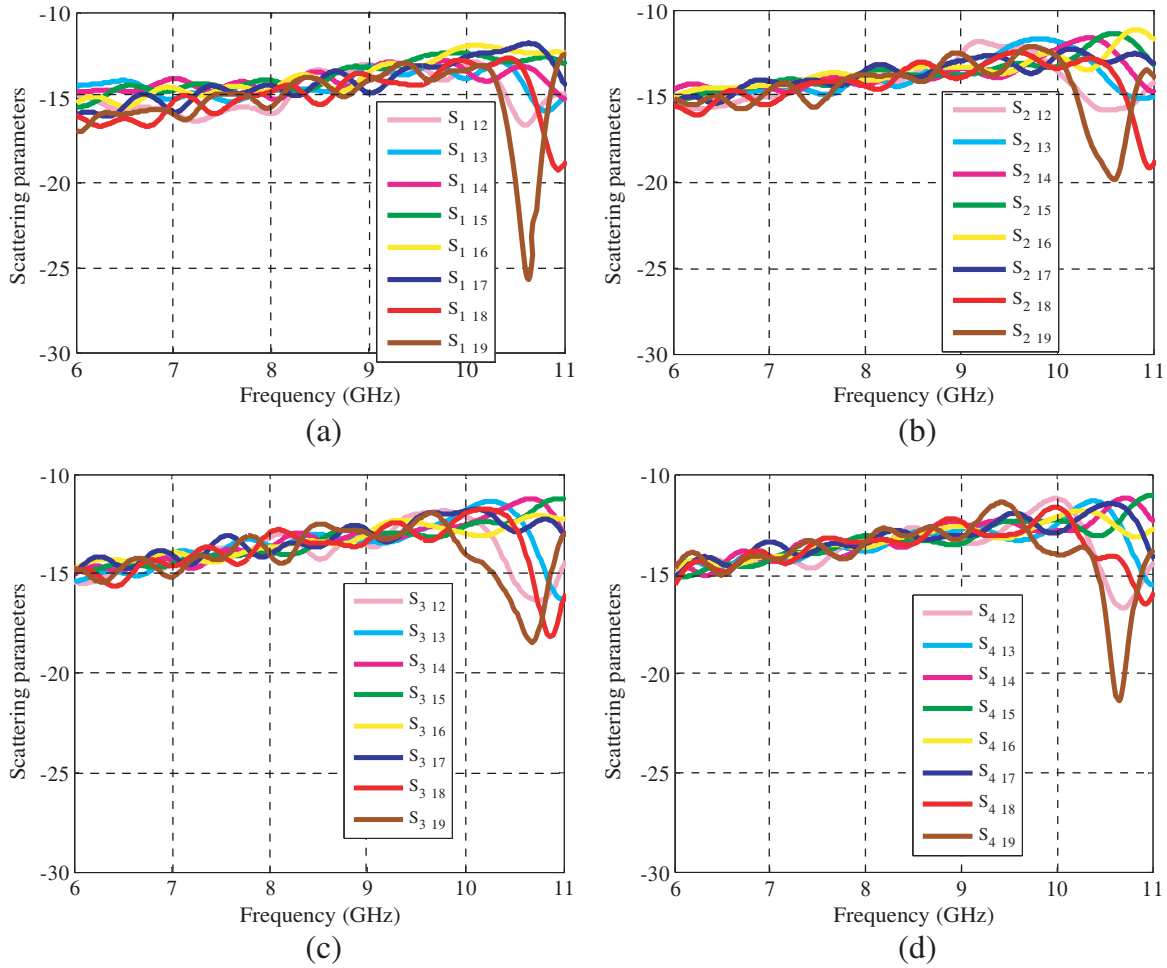


Figure 13. Full-wave simulated coupling diagram for the proposed Rotman lens: (a) ports 1 to output ports, (b) input port 2 to output ports, (c) input port 3 to output ports, (d) input port 4 to output ports. (Y scale is in dB).

simulation coupling diagrams from beam ports to array ports are presented in Fig. 13. To show the beam scanning and scan loss, the array factors for the proposed Rotman lens are normalized to the highest beam level in all frequencies (based on Full-wave s -parameters). The array factors for 6, 9, and 11 GHz are plotted in Figs. 14(a), (b), and (c), respectively. It is viewed that the beam positions do not change significantly with frequency, and their beamwidths are reduced as the frequency increases. It should be mentioned that the plotted array factors are based on full-wave scattering parameters.

Then, DRAs are selected as radiating elements in the proposed phased array antenna. The rectangle-shaped DRAs offer more design flexibility than the cylindrical shape to control the impedance bandwidth. The rectangular DRA is shown in Fig. 15. Two reasons have contributed to the increase of the impedance matching bandwidth. First, the DRA is raised above the substrate by an optimal air gap, and secondly, the DRA is excited by the bevel-shaped patch that is attached to one side of the DR and connected to the input microstrip line. The dimensions of DRA are $a = 5$ mm, $b = 11.2$ mm, and $d = 12$ mm. The reflection coefficients for the single DRA element in isolation is plotted in Fig. 16.

Then, the Rotman lens and DRA array are modeled using CST software simultaneously. The elements spacing of the rectangular DRA array is 15.5 mm to avoid the grating lobes at the upper end of the band. Simulated S_{ii} of the DRA phased array of the beam ports are shown in Fig. 17. Full-wave normalized simulated radiation patterns are plotted in Fig. 18. It is interesting to point out that the beams are approximately fixed and do not change significantly with frequency.

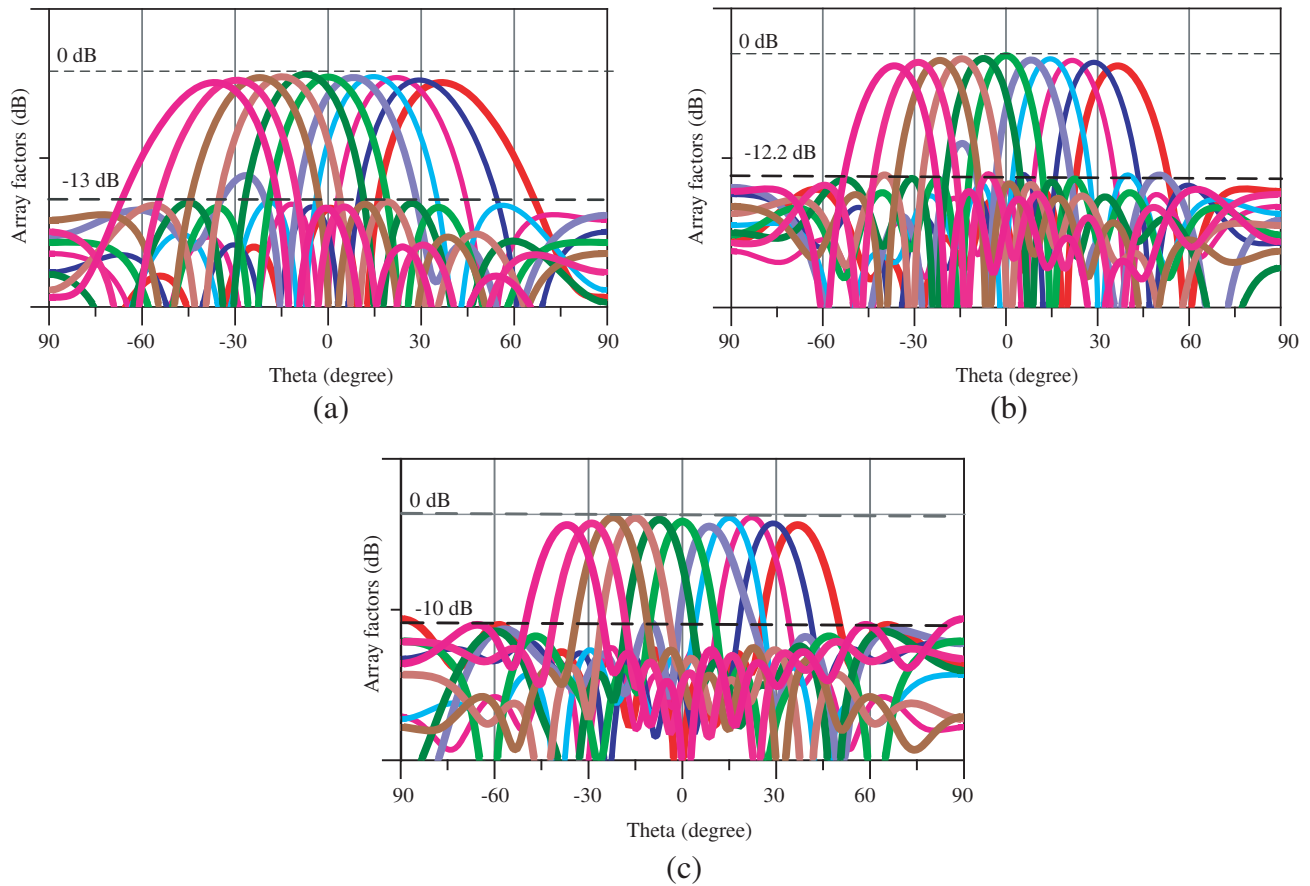


Figure 14. Rotman lens’s array factors based on full-wave *s*-parameters computation: (a) 6 GHz, (b) 9 GHz, and (c) 11 GHz.

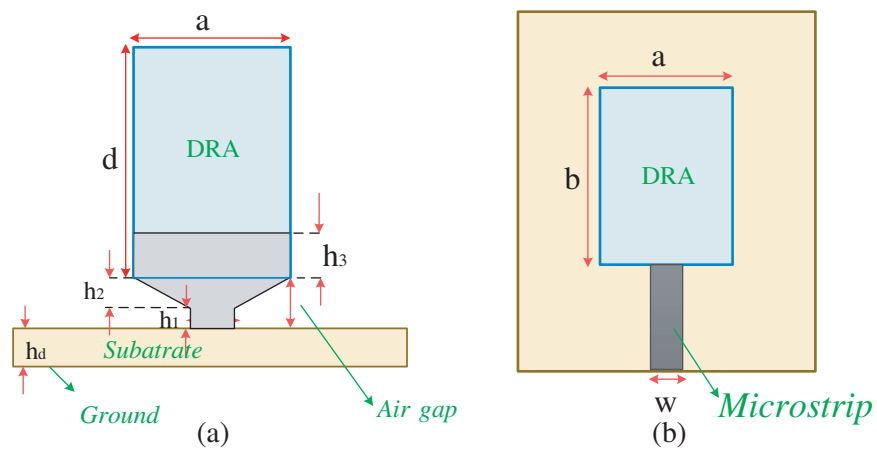


Figure 15. Geometry of the wideband dielectric resonator antenna: (a) side view, (b) top view ($h_1 = h_2 = 0.5$, $h_3 = 2.9$, $w = 1.56$, $\epsilon_{DRA} = 10.2$, $\epsilon_{sub} = 2.2$, and $h_d = 0.508$, all dimensions are in mm). The dimensions of DRA are $a = 5$ mm, $b = 11.2$ mm, and $d = 12$ mm. It should be noted that DR is placed on a gap (spacer) and the optimum gap is $h_1 + h_2 = 1$ mm.

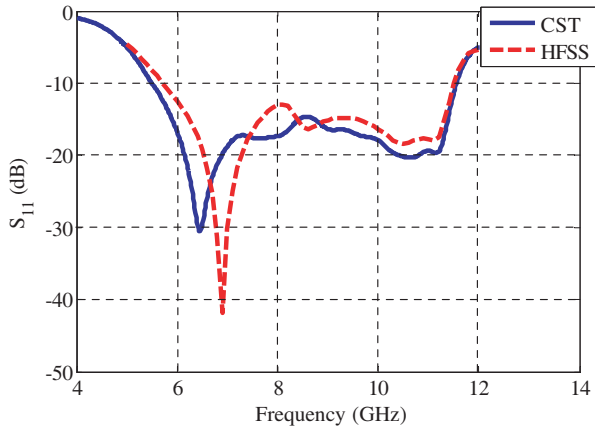


Figure 16. Full-wave simulated reflection coefficient of the proposed DRA element.

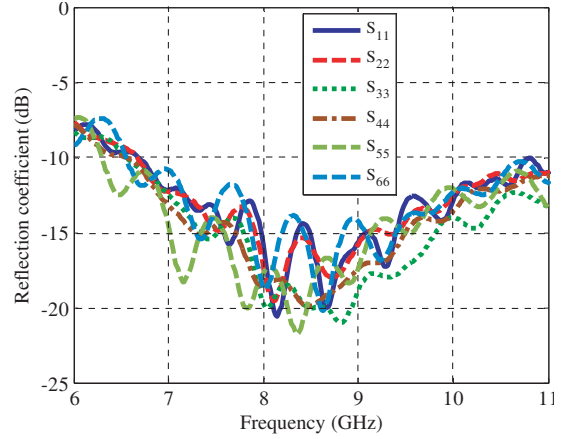


Figure 17. Reflection coefficients for the beam ports of the phased array.

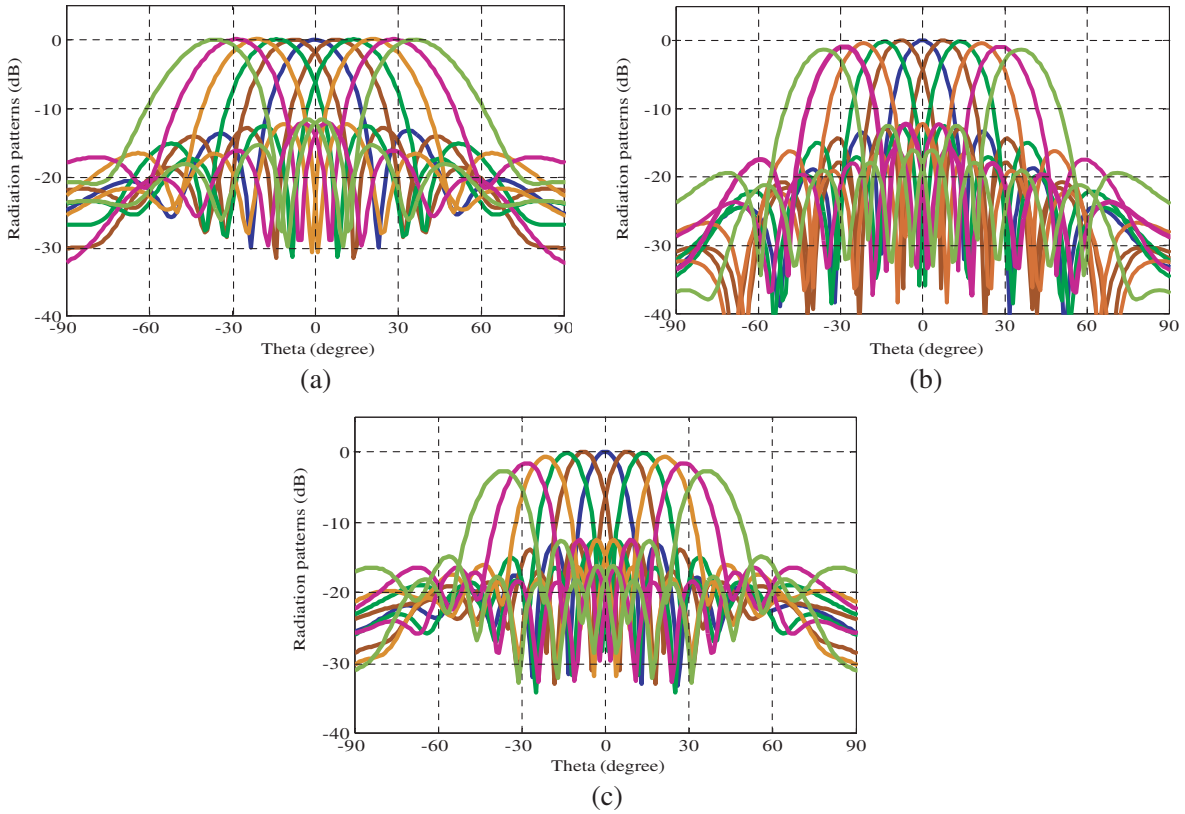


Figure 18. Full-wave simulated radiation patterns: (a) 6 GHz, (b) 9 GHz, and (c) 11 GHz.

5. CONCLUSION

A fast technique for designing the Rotman lens based on E- and H-wall symmetrical planes (like even and odd modes) has been presented. Since the Rotman lens has a challenging design procedure and to get the best results, it needs to be analyzed using full-wave simulators for several times. This technique has sped up the design process significantly. Then, wideband DRA has been used as an element of the antenna array. Such a design has provided wide-scan and wideband phased array antenna. Some prototypes have been built and tested to prove the concept.

REFERENCES

1. Rotman, W. and R. Turner, "Wide-angle microwave lens for line source applications," *IEEE Trans. Antennas Propag.*, Vol. 11, No. 6, 623–632, Nov. 1963.
2. Lambrecht, A., S. Beer, and T. Zwick, "True-time-delay beamforming with a Rotman-lens for ultrawideband antenna systems," *IEEE Trans. Antennas Propag.*, Vol. 58, No. 10, 3189–3195, Oct. 2010.
3. Archer, D. H. and M. J. Maybell, "Rotman lens development history at Raytheon electronic warfare systems 1967–1995," *Proc. IEEE AP-S Int. Symp.*, Vol. 2B, 31–34, Jul. 2005.
4. Kim, J., C. S. Cho, and F. S. Barnes, "Dielectric slab Rotman lens for micro/millimeter-wave applications," *IEEE Trans. Microw. Theory Tech.*, Vol. 53, No. 8, 2622–2627, Aug. 2005.
5. Peterson, A. F. and E. O. Rausch, "Scattering matrix integral equation analysis of the design of a waveguide Rotman lens," *IEEE Trans. Antennas Propag.*, Vol. 47, No. 5, 870–878, May 1999.
6. Chan, K. K. and S. K. Rao, "Design of a Rotman lens feed network to generate a hexagonal lattice of multiple beams," *IEEE Trans. Antennas Propag.*, Vol. 50, 1099–1108, Aug. 2002.
7. Yu, M., D. Zhao, Y. Jin, and B. Wang, "Near-field image restoration for Rotman lens by localized angle-time spread function-based filtering method," *IEEE Trans. Antennas Propag.*, Vol. 63, No. 5, 2353–2358, May 2015.
8. Ranjbar Nikkhah, M., M. Hiranandani, A. A. Kishk, and K. Wu, "Fast design of Rotman lens and its application in Rotman-DRA phased array," *Proc. IEEE APS Int. Symp.*, Vancouver, Canada, Jul. 2015.
9. Luk, K. M. and K. W. Leung, *Dielectric Resonator Antenna*, Research Studies Press, Baldock, England, 2003.
10. Petosa, A., *Dielectric Resonator Antenna Handbook*, 2–3, Artech House, Norwood, MA, USA, 2007.
11. Ranjbar Nikkhah, M., J. Rashed-Mohassel, and A. A. Kishk, "Compact low-cost phased array of dielectric resonator antenna using parasitic elements and capacitor loading," *IEEE Trans. Antennas Propag.*, Vol. 61, No. 4, 2318–2321, Apr. 2013.
12. Ranjbar Nikkhah, M., P. Loghmanni, J. Rashed-Mohassel, and A. A. Kishk, "Theory of ESPAR design with aperture coupled dielectric resonators and their implementation in large arrays," *IEEE Trans. Antennas Propag.*, Vol. 62, No. 6, 3359–3364, Jun. 2014.
13. Karabey, O. H., A. Mehmood, M. Ayluctarhan, H. Braun, M. Letz, and R. Jakoby, "Liquid crystal based phased array antenna with improved beam scanning capability," *Electronics Letters*, Vol. 50, No. 6, 426–428, Mar. 13, 2014.
14. CST Microwave Studio, ver. 2013, CST AG. D-64289 Darmstadt, Germany, 2013.
15. Chair, R., A. A. Kishk, and K. F. Lee, "Wideband simple cylindrical dielectric resonator antennas," *IEEE Microw. Wireless Comput. Lett.*, Vol. 15, No. 4, 241–243, Apr. 2005.
16. Tekkou, K., M. Ettorre, L. Le Co, and R. Sauleau, "Multibeam SIW slotted waveguide antenna system fed by a compact dual-layer Rotman lens," *IEEE Trans. Antennas Propag.*, Vol. 64, No. 2, 504–514, Feb. 2016.
17. Cheng, Y. J., W. Hong, K. Wu, Z. Q. Kuai, Y. Chen, J. X. Chen, J. Y. Zhou, and H. J. Tang, "Substrate integrated waveguide (SIW) Rotman lens and its band multibeam array antenna applications," *IEEE Trans. Antennas Propag.*, Vol. 56, No. 8, 2504–2513, Aug. 2008.
18. Lee, W., J. Kim, and Y. J. Yoon, "Compact two-layer Rotman lens-fed microstrip antenna array at 24 GHz," *IEEE Trans. Antennas Propag.*, Vol. 59, No. 2, 460–466, Feb. 2011.
19. Christie, S., R. Cahill, N. B. Buchanan, V. F. Fusco, N. Mitchell, Y. V. Munro, and G. Maxwell-Cox, "Rotman lens-based retrodirective array," *IEEE Trans. Antennas Propag.*, Vol. 60, No. 3, 1343–1351, Mar. 2012.